Detection of Active Wildland Fires Using Multitemporal MODIS Images

Keiji Kushida

***Abstract*—The fire fractional area and radiances at 4 and 11 μm of active fires in the boreal forests in Siberia and Mongolia were estimated using Advanced Spaceborne Thermal Emission and Reflection Radiometer images. In addition, a stochastic fire model was constructed. The efficiency of a biband threshold method used for detecting active fires on the basis of the thermal anomaly obtained from multitemporal Moderate Resolution Imaging Spectroradiometer (MODIS) images was evaluated using the stochastic fire model. The simulation results of fire detection indicated that the aforementioned method accurately detected 80% of the fire pixels with false alarms that were less than 2×10^{-5} when the radiances of the nonfire pixels at 4 and 11 μm were estimated using past MODIS images with a standard deviation (SD) of 1 K. The analyses also indicated that, in order to obtain fewer errors than those obtained using the conventional contextual algorithm (MOD14) from the objective area (omission errors that are less than 62% and commission errors that are less than 2×10^{-5}), it is essential to carry out the nonfire radiance estimation using past images with an SD of less than 3 K. During an actual application of the multitemporal method to several fire cases, fewer errors occurred than those that occurred using MOD14.**

***Index Terms*—Fire detection, infrared, Moderate Resolution Imaging Spectroradiometer (MODIS), stochastic modeling.**

I. Introduction

ACTIVE-FIRE detection, fire-spread prediction, and appropriate fire suppression are essential for restricting the expansion of fire.

A contextual fire-detection algorithm [1] is used for developing Moderate Resolution Imaging Spectroradiometer (MODIS) fire product version 4 (MOD14). The contextual fire-detection algorithm was evaluated in Siberia [2], the U.S. [3], southern Africa [4], and Brazil [5], [6]. Comparisons with Advanced Spaceborne Thermal Emission and Reflection Radiometer (ASTER) onboard the Earth Observing System (EOS) Terra suggested that the commission errors of MODIS active-fire detection (false alarms per nonfire area) were small—3% in Brazil [6] and 3% in Siberia [2]—while omission errors were more common, particularly for small fires. MODIS had a 50% detection rate when fire activity was observed in an ASTER image as a 0.04-km^2 cluster in Brazil [5], 0.03-km^2 cluster in southern Africa [4], and 0.05-km^2 cluster in Siberia [2].

Because the present operational algorithm was based on fire detection with a single-date image, there was a need to develop a multitemporal approach based on the detection of an anomalous change, which has great potential for developing future advanced fire-detection algorithms. Most recently, the multitemporal approach was tested for MODIS fire detection [7]. Cloud-removed nonfire background radiances of a current image at respective 4 and 11 μm were estimated with root-mean-square errors (rmses) of 0.5–2.0 K and 0.5–1.5 K using past multitemporal MODIS images. However, the relationship between the error of the background radiance estimation and the fire-detection error has not been studied, and the acceptable error levels in the estimated background radiance, which is essential for developing a more reliable fire-detection algorithm than the contextual single-date algorithm, have not been determined.

In this letter, I first determine the distribution of fire characteristics such as fire fractional area and thermal radiance of the active fire and background pixels in the boreal forests in Siberia and Mongolia using ASTER images. Second, I evaluate active-fire detection with the simulated multitemporal MODIS images using biband thresholds based on a stochastic model of fire and the estimated error levels of background radiances. Third, I test fire detection in actual cases by comparing with MOD14. Daytime images are used for the study.

II. Stochastic Fire Model

A. ASTER and MODIS Images

The study areas were the boreal forests in Siberia and Mongolia. Table I shows the fire scenes used in constructing the stochastic fire model (scenes A–E) and the fire scenes used in evaluating fire detection (scenes F–I). The burnt area was calculated as the cumulative area up until the time of the satellite overpass by tracing the fire scars in the ASTER images. The Siberian study area (scenes except for C) was dominated by larch, pine, and birch forests. The Mongolian study area (scene C) was dominated by larch, pine, and birch forests and grassland. All of the fires occurred in the forest.

ASTER was used for evaluating the fire characteristics in the boreal forests in Siberia and Mongolia. It has been used for the validation of fire-detection algorithms in previous studies [2], [4]–[6]. One pixel of MODIS is usually larger than the size of a burning area at a given time. With the use of fine-resolution sensors such as ASTER, the fractional area and spread of fire can be identified and analyzed. Table II shows the corresponding wavelengths of MODIS and ASTER. ASTER and MODIS have bands at 2.1–2.2 and 10–12 μm; however, MODIS only has bands near 4 μm. The 4- and 10–12-μm bands are important in the MOD14 algorithm. From the ASTER bands at 1.65, 2.165, and 11.3 μm and the MODIS band at 4.0 μm, which was acquired on the same day as the ASTER image,

Manuscript received November 21, 2008; revised April 21, 2009. Date of publication January 15, 2010; date of current version April 14, 2010. This work was supported by Scientific Research (C) (90291236) from the Ministry of Education, Culture, Sports, Science and Technology, Japan.

The author is with the Center for Far Eastern Studies, University of Toyama, Toyama 930-8555, Japan (e-mail: kkushida@sci.u-toyama.ac.jp).

Digital Object Identifier 10.1109/LGRS.2009.2034029

TABLE I
FIRE USED IN ANALYSIS

MODIS/ ASTER image	Latitude	Longitude	Burnt area (km^2)	Burning area (km^2)	Date	MODIS acquisition time (GMT)	ASTER acquisition time (GMT)	ASTER image average temperature[a] (K)
A	55°22' N	115°27' E	39.8	0.93	7 July 2006	3:35	3:37	296.4
B	52°51' N	113°50' E	3.9	0.53	8 July 2004	3:40	3:44	303.8
C	48°48' N	112°17' E	98.6	0.88	30 June 2006	3:30	3:33	303.1
D	63° 9' N	124°21' E	332.8	7.67	1 August 2002	3:15	3:12	289.4
E	64°11' N	125° 8' E	44.2	0.16	1 August 2002	3:15	3:12	292.3
F	61° 9' N	124°49' E	21.0	0.11	23 July 2002	3:15	3:19	296.9
G	61°40' N	125°13' E	32.2	0.45	23 July 2002	3:15	3:18	297.0
H	62°40' N	125°58' E	235.5	7.05	23 July 2002	3:15	3:18	296.5
I	63°11' N	126°29' E	41.3	2.02	23 July 2002	3:15	3:18	295.7

[a]Cloud mask was excluded.

TABLE II
MODIS AND ASTER WAVELENGTHS FOR FIRE DETECTION

MODIS			ASTER		
Band	Wavelength (μm)	Resolution (m)	Band	Wavelength (μm)	Resolution (m)
	–		4	1.600~1.700	30
7	2.105~2.155	500	5	2.145~2.185	30
21&22	3.929~3.989	1000		–	
31	10.78~11.28	1000	14	10.95~11.65	90

TABLE III
RADIANCES AT 11.3 μm FOR THE BACKGROUNDS OF THE MODIS FIRE PIXEL AND THE SCENE [W/(m^2 · sr · μm)]

Scene	Background of the fire pixel	Background of the scene
A	9.75 ± 0.40	8.91 ± 0.63
B	10.50 ± 0.39	10.27 ± 0.48
C	10.92 ± 0.38	10.14 ± 1.14
D	9.23 ± 0.64	8.67 ± 1.00
E	8.85 ± 0.13	8.77 ± 0.84

the radiance at 4.0 μm in the ASTER images was estimated by following [8]. Kushida *et al.* [8] assumed that a small portion of the burning area (f) has a high temperature (T_h) and that the remaining wide area $(1-f)$ has a considerably low temperature (T_c) by following [9], calculated T_h and f from the spectral radiance equations at 1.65, 2.165, and 11.3 μm, and obtained the radiance at 4.0 μm from T_h and f. The radiance at 1.65 μm contributed to estimating the reflected solar radiance at 2.165 μm. MODIS and ASTER are onboard the same EOS Terra platform.

Following the previous study [10], active-fire pixels in the ASTER images were detected. The fire pixels were treated as a burning area, and the fraction of fire spread in every 990 m × 990 m area (33 × 33 pixels), which is equivalent to one pixel of MODIS, in the ASTER images was calculated and defined as the fire fractional area. The fire pixel does not entirely correspond to the burning place; however, the treatment is useful for constructing a fire stochastic model. The radiance averages of the burning area of each MODIS fire pixel, the background of each MODIS fire pixel, and the background of the scenes at 11 and 4 μm were calculated. The estimations of the radiances at 4 μm for both of the fire and nonfire MODIS pixels were accurate with the coefficient of determination $R^2 = 0.70$ from the evaluation with the MODIS images [8]. A stochastic fire model that describes the relationship between the fire fractional area in one MODIS pixel and the radiances of the burning area and backgrounds of the fire pixels at 4 and 11 μm was constructed on the basis of the relationships between them, which were observed in actual fire cases. The model also described the distribution of the aforementioned parameters. Some 195 samples of the MODIS fire pixel and 30 251 samples of the MODIS nonfire pixel in the five scenes were used for constructing the stochastic fire model.

B. Stochastic-Fire-Model Parameterization

The Kolmogrov statistical test showed that the fire fractional area (F[m^2/m^2]) and the radiance of the burning area of the fire pixel at 11 μm (R_{11} [W/(m^2 · sr · μm)]) and 4 μm (R_4 [W/(m^2 · sr · μm)]) obeyed lognormal distributions, respectively. I assumed lognormal distributions for each of the three variables and obtained the following:

$$\ln F \sim N(-3.87, 1.45^2) \quad (1)$$
$$\ln R_{11} \sim N(2.48, 0.117^2) \quad (2)$$
$$\ln R_4 \sim N(2.47, 0.745^2). \quad (3)$$

Here, $N(\mu, \sigma^2)$ denotes the normal distribution with mean μ and variance σ^2. The coefficients of correlations between $\ln F$ and $\ln R_{11}$, $\ln F$ and $\ln R_4$, and $\ln R_4$ and $\ln R_{11}$ were 0.71, 0.73, and 0.84, respectively. I assumed that the distribution of $\ln F$, $\ln R_4$, and $\ln R_{11}$ was a 3-D normal distribution with the aforementioned parameters.

Table III shows the radiances of the background of the scene ($\overline{R_{b11}}$ [W/(m^2 · sr · μm)]) and the background of the MODIS fire pixel ($\overline{R_{\mathrm{bf11}}}$ [W/(m^2 · sr · μm)]) at 11 μm averaged over the scene. The relationship between the two is expressed as follows:

$$\overline{R_{\mathrm{bf11}}} = \overline{R_{b11}} + 0.498, \quad R^2 = 0.85. \quad (4)$$

The higher values of $\overline{R_{\mathrm{bf11}}}$ than that of $\overline{R_{b11}}$ may be caused by smoldering areas near the burning areas identified in the ASTER image. No significant correlations between the radiances of the burning area and the background of the MODIS fire pixel were found. By adding the variance of $\overline{R_{\mathrm{bf11}}}$ as the average value of the five scenes, we obtain

$$R_{\mathrm{bf11}} \sim \overline{\overline{R_{b11}}} + 0.498 + 0.388N(0,1). \quad (5)$$

Here, $R_{\mathrm{bf}11}$ [W/(m^2 · sr · μm)] denotes the background of the MODIS fire pixel at 11 μm, and $\overline{\overline{R_{b11}}}$ [W/(m^2 · sr · μm)]) denotes the background radiances of the pixel at 11 μm, estimated by the multitemporal MODIS images before the occurrence of fire. From the regression observed in the five scenes, the relationship between the radiances of the background of the scene at 11 μm (R_{b11} [W/(m^2 · sr · μm)]) and 4 μm (R_{b4} [W/(m^2 · sr · μm)]) is expressed as follows:

$$R_{b4} = 0.212R_{b11} - 1.16, \quad R^2 = 0.69. \tag{6}$$

By assuming that (6) holds for those of the background radiances of the pixel at 4 μm, estimated by the multitemporal MODIS images before the occurrence of fire ($\overline{\overline{R_{b4}}}$ [W/(m^2 · sr · μm)]) and $\overline{\overline{R_{b11}}}$ and those of the background of the fire pixel at 4 μm ($R_{\mathrm{bf}4}$ [W/(m^2 · sr · μm)]) and $R_{\mathrm{bf}11}$, we obtain from (5)

$$R_{\mathrm{bf}4} \sim \overline{\overline{R_{b4}}} + 0.106 + 0.0823N(0,1). \tag{7}$$

The radiances of the fire pixel at 11 μm (P_{11} [W/(m^2 · sr · μm)]) and 4 μm (P_4 [W/(m^2 · sr · μm)]) were assumed to be a linear mixture of those of the burning area and background of the pixel, and they are expressed as follows:

$$P_{11} = FR_{11} + (1-F)R_{\mathrm{bf}11} \tag{8}$$

$$P_4 = FR_4 + (1-F)R_{\mathrm{bf}4}. \tag{9}$$

III. Biband Threshold Method

The estimated background radiance is defined as the cloud-removed nonfire radiance of the image at the time of detection estimated from past multitemporal MODIS images. The estimated background radiance was compared with the radiance at a detection time, and the thermal anomaly (TA) was detected in the image. The difference between the observed radiance at a detection time and the estimated background radiance was defined as TA. The joint probability density distribution of TA at 4 and 11 μm (TA_{11}, TA_4) was determined for both the fire and nonfire pixels using a 0.05 W/(m^2 · sr · μm) × 0.05 W/(m^2 · sr · μm) grid cell. The stochastic fire model shown in (1)–(9) was used to simulate 10^8 fire and 10^8 nonfire pixels using pseudorandom numbers.

Assuming that the probability density distributions of both background radiances at a detection time ($R_{\mathrm{db}11}, R_{\mathrm{db}4}$) and the estimated background radiances ($R_{\mathrm{eb}11}, R_{\mathrm{eb}4}$), respectively, are 2-D normal distributions expressed using the regression equation (6), the distribution of TA $[(TA_{\mathrm{b}11}, TA_{b4}) = (R_{\mathrm{db}11}, R_{\mathrm{db}4}) - (R_{\mathrm{eb}11}, R_{\mathrm{eb}4})]$ obeys a 2-D normal distribution with two eigenvectors $(1/\sqrt{1^2 + 0.212^2})(1, 0.212)$ and $(1/\sqrt{1^2 + 0.212^2})(-0.212, 1)$ in the case of nonfire pixels with the average of TA $(\overline{TA_{b11}}, \overline{TA_{b4}})$ of (0, 0). Furthermore, the standard deviations (SDs) of TA at 4 and 11 μm (SD(TA_{b11}), SD(TA_{b4})) were assumed to be $k(0.136, 0.0276)$ [W/(m^2 · sr · μm)] ($k = 1, 2, 3$). These values correspond to the difference in radiances by 1, 2, and 3 K when the temperature value is 300 K from the Planck equation. In the range of cloud-removed nonfire surface temperatures, these constant values are close approximations to the radiance differences. In the case of fire pixels, when the estimated background radiance was provided, the radiance at a detection time was calculated using (1)–(3), (5), and (7)–(9).

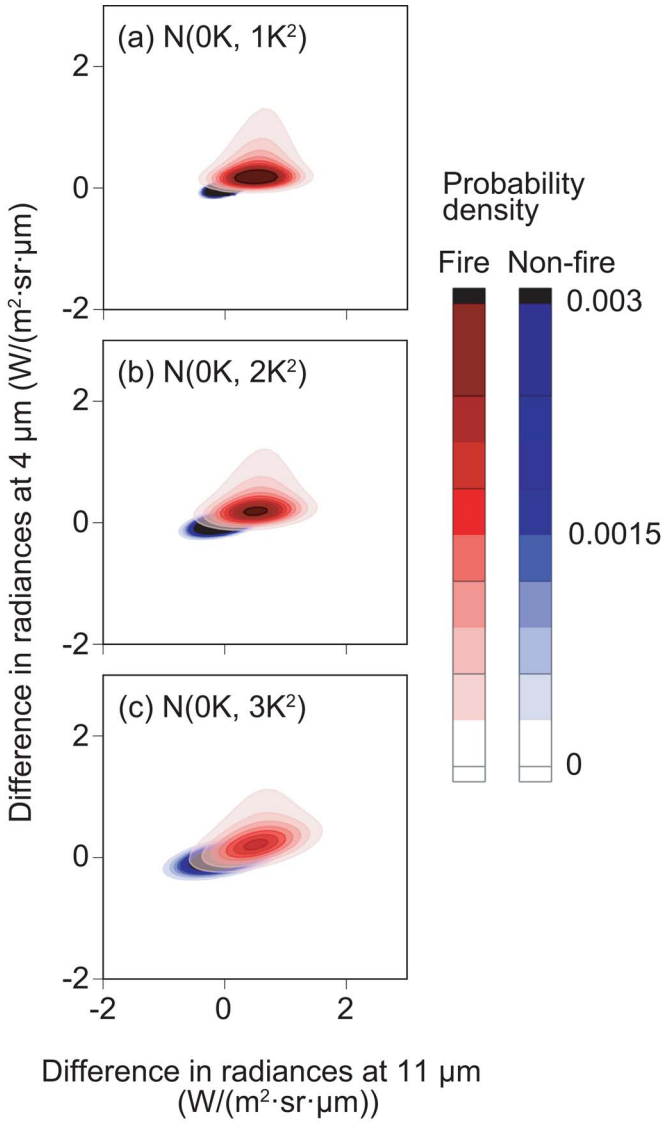

Fig. 1. Joint probability density distributions of TA at 4 and 11 μm for fire and nonfire pixels under the assumption of background TA estimation. The SDs are (a) 1 K, (b) 2 K, and (c) 3 K, and the average is 0 K.

Fig. 1 shows the joint probability density distributions of TA at 4 and 11 μm in the case of fire and nonfire pixels under the assumption that the SDs are 1, 2, and 3 K and the average is 0 K. The red and blue colors indicate the fire and nonfire pixels, respectively. The first principal component axes of the fire and nonfire pixel distributions were at an angle. This is because, at a high temperature, the radiance at 4 μm is more intense as compared to that at 11 μm. The distributions of the nonfire and fire pixels broadened with an increase in SD.

Cost function [C (in percent)] is defined as follows [11]:

$$C = w_o E_o + w_c E_c \tag{10}$$

where E_o and E_c (in percent) denote the omission and commission errors of fire detection, respectively, and w_o and w_c denote the weights assigned to E_o and E_c, respectively. In general, the number of nonfire pixels is greater than that of fire pixels in a satellite scene. In this case, w_c should be larger than w_o to

TABLE IV
OMISSION ERRORS (IN PERCENT) AND COMMISSION ERRORS [PER(10^6-km^2 NONFIRE AREA)] OBTAINED IN ACTIVE-FIRE DETECTION UNDER THE ASSUMPTIONS OF TA DISTRIBUTION OF NONFIRE PIXELS (THE COMMISSION ERROR IS SHOWN IN THE PARENTHESIS)

		Actual TA distribution					
		N(0K,0.5K^2)	N(0K,1K^2)	N(0K,1.5K^2)	N(0K,2K^2)	N(0K,2.5K^2)	N(0K,3K^2)
Predicted TA distribution	N(0K,1K^2)	16 (0)	16 (18)	16 (5.7×10^3)	26 (4.9×10^4)	15 (1.4×10^5)	15 (2.5×10^5)
	N(0K,2K^2)	50 (0)	49 (0)	48 (0)	47 (20)	45 (9.0×10^2)	43 (6.9×10^3)
	N(0K,3K^2)	63 (0)	63 (0)	63 (0)	63 (0)	62 (1)	61 (19)

Soild square shows that the omission error is less than 62% and the commission error is less than $20/(10^6\,\text{km}^2$ non-fire).

minimize the number of misclassified pixels. Weight (W) is defined as

$$W = \frac{w_c}{w_o}. \tag{11}$$

In the setting of the thresholds, a single straight line on the scatter plot of TA at 4 and 11 μm (TA_{11}, TA_4) was not used as a threshold, but a grid-by-grid threshold setting was used. This method follows the maximum-likelihood method. When $W = 1$, if the probability density of TA of the fire pixel is larger than that of the nonfire pixel in a grid cell $d(i, j)$ on the scatter plot of TA at 4 and 11 μm (TA_{11}, TA_4), then the pixels whose TA ranged in $d(i, j)$ are classified as fire pixels, and if the probability density of TA of the fire pixel is smaller than that of the nonfire pixel, then those pixels are classified as nonfire pixels. The summation of the probability densities of the fire pixels in $d(i, j)$ that correspond to the classified nonfire pixels is defined as omission error, and the summation of the probability densities of nonfire pixels in $d(i, j)$ that correspond to the classified fire pixel is defined as commission error. When $W > 1$, the probability density of TA of the fire pixel is divided by W and compared with that of the nonfire pixel. The omission and commission errors are calculated in a similar way. W was first set to one, and it was increased one by one until the commission errors reached less than 2.0×10^{-5}.

So far, the distribution of the actual TA was assumed as the same as that of the predicted one. When the actual and predicted radiance values differ, the threshold setting is based on the predicted distribution, and the estimation of the omission and commission errors is based on the actual distribution. Several cases were tested in which the predicted and actual distributions were different. The aforementioned assumptions were adopted for determining the actual distribution, and for each of the cases, the predicted distribution was similarly assumed with the parameters of the background TA distribution, the SDs of 0.5, 1, 1.5, 2, 2.5, and 3 K, and the average of 0 K.

Table IV shows the omission and commission errors obtained during active-fire detection. The unit of the commission error in Table IV was defined as the number of false alarms per 10^6-km^2 nonfire area in the MODIS image. During the evaluation of the omission and commission errors, the condition when the omission error was less than 62% and the commission error was less than $20/(10^6$-km^2 nonfire area) was treated as a standard. It was reported in a previous paper [2] that the commission error obtained by carrying out the MOD14 algorithm was 2.1×10^{-5} in Siberia. The omission error obtained by carrying out the MOD14 algorithm was estimated at 62% from the relationship between the omission error and the number of ASTER fire pixels in a MODIS pixel (NF) [2] and the NF distribution obtained in this paper.

When the SD of the actual background TA distribution was 0.5 K–1 K, 84% of the fire pixels were correctly detected with less than $18/(10^6$-km^2 nonfire area) false alarms with the use of the predicted distribution N (0 K, 1 K^2). The use of N (0 K, 2 K^2) as the predicted distribution resulted in the generation of a lesser number of errors than the standard number when the SD of the actual background TA distribution was 0.5–2 K. When the SD of the actual distribution was 2.5–3 K, the use of N (0 K, 3 K^2) as the predicted distribution resulted in the generation of a number of errors that were less than the standard number. When the SD of the actual background TA was greater than that of the predicted background TA, a larger number of commission errors were generated than the standard number.

IV. FIRE DETECTION USING MODIS

Multitemporal active-fire detection was applied to real MODIS data and evaluated with MOD14. The MODIS L1B and MOD14.5 data in the range of $60°-63°30'$ N and $123°-130°$ E (approximately 400 km $\times$ 400 km area) acquired at 3:00 GMT on July 18, 2002, and at 3:15 GMT on July 23, 2002, were downloaded from the Level 1 and Atmosphere Archive and Distribution System and Land Processes Distributed Active Archive Center sites. The fire pixels detected by MOD14 in the image on July 18, 2002, and the cloud and water areas detected by the cloud and water masks of MOD14 in the images on both days were excluded from the analysis.

The linear regression equations were obtained for estimating the radiances at 4 and 11 μm in the pixel in the image on July 23, 2002 (T_{11-1} [W/(m^2 · sr · μm)], T_{4-1} [W/(m^2 · sr · μm)]) from the radiances at 4 and 11 μm in the pixel at the same location in the image on July 18, 2002 (T_{11-0}[W/(m^2 · sr · μm)], T_{4-0} [W/(m^2 · sr · μm)]) using all the pixels. The differences between (T_{11-1}, T_{4-1}) and the estimated (T_{11-1}, T_{4-1}) were treated as TA. The multitemporal fire detection shown in III was operated with N (0 K, 2.9 K^2) as the predicted background TA distribution. The pixels detected as fire were removed from the data set, and the regression equation was recalculated until there were no pixels to remove. The calculation was finished after the three repeats. The rmses of regression at 4 and 11 μm were 2.3 and 2.6 K, respectively. The regression equations are as follows:

$$T_{11-1} = 0.691T_{11-0} - 0.159T_{4-0} + 3.06 \tag{12}$$

$$T_{4-1} = 0.171T_{11-0} - 0.0391T_{4-0} - 0.798. \tag{13}$$

The ASTER images shown in Table I scenes F–I were overlaid in the MODIS images and were used for the evaluation of active-fire detection. Active fires were detected in the ASTER images, as shown in II, and MODIS pixels that include these active fires were treated as "true" fire pixels. If a fire was detected by one algorithm in one "true" fire, it was counted as correctly detected. Otherwise, it was counted as an omission error. If one algorithm detected fires where there were no "true" fires in the eight-neighborhood, it was counted as a commission error. Table V shows the omission errors obtained during the multitemporal algorithm and MOD14. There were no

TABLE V
OMISSION ERRORS IN MODIS FIRE DETECTION

	Number of	Multitemporal		MOD14	
	"True" fire pixels	Number of pixels	Rate	Number of pixels	Rate
F	5	3	60%	3	60%
G	28	16	57%	15	54%
H	113	44	39%	82	73%
I	29	6	21%	17	59%
Total	175	69	39%	117	67%

commission errors detected by both algorithms. The omission error rate obtained during the multitemporal algorithm was 39%, while that obtained during MOD14 was 67%. The omission errors obtained during the multitemporal algorithm were smaller than those obtained during MOD14 on the fire lines along the straight-through edges of the large fire scars, which appeared in scenes H and I.

When the TA distributions of fire and nonfire pixels were treated as actual distributions, results revealed that the omission and commission errors were 61% and $0/(10^6\text{-km}^2$ nonfire area), respectively. These values were equivalent to or smaller than 60% and $20/(10^6\text{-km}^2$ nonfire area), respectively, which were obtained by assuming TA background distributions as N (0 K, 2.9 K^2). Since the rmses of regression at 4 and 11 μm were 2.3 and 2.6 K, respectively, the disparity of the background TA distribution from the normal distribution was compensated by increasing SD by 0.3–0.6 K.

V. DISCUSSIONS AND CONCLUSION

A stochastic fire model that estimates the fire fractional area and radiances at 4 and 11 μm of the active fire in the boreal forests in Siberia and Mongolia using ASTER images has been constructed. This model was used to evaluate the biband threshold method for detecting active fires on the basis of the TA distribution obtained from multitemporal MODIS images. The omission and commission errors were dependent on the estimation errors of the cloud-removed nonfire background radiances of the image at a detection time at 4 and 11 μm derived from past multitemporal images. Assuming that the error function was a 2-D normal distribution, it was found that 80% of the fire pixels were correctly detected with false alarms that were less than 2×10^{-5} when the background radiances at 4 and 11 μm were estimated from past MODIS images with an SD of 1 K. It was essential to carry out the cloud-removed nonfire radiance estimation using past images with an SD of less than 3 K to obtain an omission error of less than 62% and a commission error of less than 2×10^{-5}; this technique ensured the generation of a fewer number of errors than that generated by MOD14. During an actual application of the multitemporal method to several fire cases in Siberia, fewer errors occurred than those that occurred using MOD14. The multitemporal method had an advantage over MOD14, particularly on the fire lines along the straight-through edges of the large fire scars.

Koltunov and Ustin [7] has estimated the background radiances at respective 4 and 11 μm with the SDs of the error of 0.5–2.0 K and 0.5–1.5 K and the average of the error of approximately 0 K using multitemporal MODIS images in northern California. In more than half of the tested cases at 4 and 11 μm, the SD was less than 1.0 K. The result of our study indicates that the method [7] is effective in estimating background radiances for detecting the active fire. However, in the method [7], 27 past multitemporal MODIS images chosen from 556 images were used to estimate the background radiances of the image at a detection time. The procedure was computationally more demanding than that of MOD14. This paper indicates that the technique presented in this paper with a simple procedure of the background radiance estimation that provides an SD of less than 3 K could extract active fires more accurately than MOD14.

The stochastic models for determining the fire fractional area and radiances at 4 and 11 μm of active fires are presumably dependent on the fire characteristics of the place of occurrence. In order to detect fire using multitemporal images, an appropriate stochastic model of the burning area specific to the region or fire type is indispensable. Therefore, it is essential to accumulate stochastic fire information using the aforementioned technique.

Since the multitemporal and contextual techniques are based on different procedures for fire detection, intercomparison and combination between them have possibilities for further improving the technique of fire detection.

ACKNOWLEDGMENT

The author would like to thank S. C. Liew of the National University of Singapore and the anonymous reviewers for their valuable suggestions.

REFERENCES

[1] L. Giglio, J. Descloitres, C. O. Justice, and Y. J. Kaufman, "An enhanced contextual fire detection algorithm for MODIS," *Remote Sens. Environ.*, vol. 87, no. 2/3, pp. 273–282, Oct. 2003.

[2] I. A. Csiszar, J. T. Morisette, and L. Giglio, "Validation of active fire detection from moderate-resolution satellite sensors: The MODIS example in northern Eurasia," *IEEE Trans. Geosci. Remote Sens.*, vol. 44, no. 7, pp. 1757–1764, Jul. 2006.

[3] T. J. Hawbaker, V. C. Radeloff, A. D. Syphard, Z. Zhu, and S. I. Stewart, "Detection rates of the MODIS active fire product in the United States," *Remote Sens. Environ.*, vol. 112, no. 5, pp. 2656–2664, May 2008.

[4] J. T. Morisette, L. Giglio, I. Csiszar, and C. O. Justice, "Validation of the MODIS active fire product over Southern Africa with ASTER data," *Int. J. Remote Sens.*, vol. 26, no. 19, pp. 4239–4264, Oct. 2005.

[5] J. T. Morisette, L. Giglio, I. Csiszar, A. Setzer, W. Schroeder, D. Morton, and C. O. Justice, "Validation of MODIS active fire detection products derived from two algorithms," *Earth Interact.*, vol. 9, no. 9, pp. 1–25, Jul. 2005.

[6] W. Schroeder, E. Prins, L. Giglio, I. Csiszar, C. Schmidt, J. Morisette, and D. Morton, "Validation of GOES and MODIS active fire detection products using ASTER and ETM+ data," *Remote Sens. Environ.*, vol. 112, no. 5, pp. 2711–2726, May 2008.

[7] A. Koltunov and S. L. Ustin, "Early fire detection using nonlinear multitemporal prediction of thermal imagery," *Remote Sens. Environ.*, vol. 110, no. 1, pp. 18–28, Sep. 2007.

[8] K. Kushida, S. C. Liew, O. Mishigdorj, K. Kaku, M. Fukuda, and T. Honma, "A stochastic fire detection model in 4 μm constructed by using ASTER and MODIS," *Asian J. Geoinf.*, vol. 8, no. 3, pp. 19–27, Jul. 2008.

[9] M. J. Wooster and T. Kaneko, "Testing the accuracy of solar-reflected radiation corrections applied during satellite shortwave infrared thermal analysis of active volcanoes," *J. Geophys. Res.*, vol. 106, no. 7, pp. 13 381–13 393, Jul. 2001.

[10] L. Giglio, I. Csiszar, A. Restas, J. T. Morisette, W. Schroeder, D. Morton, and C. O. Justice, "Active fire detection and characterization with the Advanced Spaceborne Thermal Emission and Reflection Radiometer (ASTER)," *Remote Sens. Environ.*, vol. 112, no. 6, pp. 3055–3063, Jun. 2008.

[11] S. C. Liew, A. Lim, and L. K. Kwoh, "A stochastic model for active fire detection using the thermal bands of MODIS data," *IEEE Geosci. Remote Sens. Lett.*, vol. 2, no. 3, pp. 337–341, Jul. 2005.